Self-generation of megagauss magnetic fields during the expansion of a plasma

C. Thaury, P. Mora, A. Héron, and J. C. Adam
Centre de Physique Théorique, Ecole Polytechnique, CNRS, 91128 Palaiseau, France
(Received 4 December 2009; revised manuscript received 13 April 2010; published 27 July 2010)

The expansion of a plasma slab into a vacuum is studied using one-dimensional and two-dimensional particle-in-cell simulations. As electrons transfer their longitudinal kinetic energy to ions during the expansion, the electron temperature becomes anisotropic. Once this anisotropy exceeds a threshold value, it drives the Weibel instability, leading to magnetic fields in the megagauss range. These fields induce energy transfer between the longitudinal and transverses directions, which influences the expansion. The impact of a cold electron population on this phenomenon is also investigated.

DOI: 10.1103/PhysRevE.82.016408 PACS number(s): 52.35.−g, 52.38.Fz, 52.38.Kd, 52.65.Rr

Plasma expansion is a fundamental process which occurs in very different fields, such as astrophysics [1,2], laser-plasma ion acceleration [3–5] and thin-film deposition [6]. This phenomenon is usually described by simple one-dimensional models [7–9]. Yet, even when the system is translation-invariant along the plasma surface, several effects (e.g., Coulomb collisions [10]) can induce momentum transfer between the longitudinal and transverse directions. The purely one-dimensional (1D) description is thus, in general, inaccurate. In this paper, we show that self-generated magnetic fields can lead to such momentum transfer during the expansion of a collisionless plasma slab. This study is of particular interest in the context of laser-plasma ion acceleration, where an intense laser pulse is focused on a thin foil to create a hot electron population that transfers progressively its energy to ions via the ambipolar electric field at the plasma surface [11].

We assume here that the electron distribution is initially Maxwellian with an isotropic temperature. As the plasma expands, the longitudinal temperature $T_\parallel$ decreases and the anisotropy parameter $A=T_\perp/T_\parallel-1$ increases, which eventually leads to the growth of the Weibel instability [12–18]. The most unstable modes are obtained for $\boldsymbol{k}=k_x\boldsymbol{e}_x$, where $\boldsymbol{e}_x$ is a unit vector normal to the plasma surface. In this case, the maximum unstable wave vector is

$$k_x^m = \sqrt{A}(\omega_{pe}/c), \tag{1}$$

where ω_{pe} is the plasma frequency [12] [Fig. 1(a)]. A more general expression for $\boldsymbol{k}^m$ can be obtained from the linear dispersion relation, considering that $\boldsymbol{k}=(k_x,k_y,0)$ makes an angle θ with $\boldsymbol{e}_x$ [19]. The result depends on the orientation of the magnetic field $\boldsymbol{B}$ which can grow either along the z-axis, or in the $(\boldsymbol{e}_x,\boldsymbol{e}_y)$ plane (B_θ field). In Fig. 1(b), we observe that, in both cases, k_x^m decreases with θ faster than cos θ. This means that the largest $\boldsymbol{k}^m$ are obtained for $\theta=0$. We notice however that for small angles $k_x^m(\theta)\approx k_x^m(0)$, for both orientations of $\boldsymbol{B}$.

To study the growth of the Weibel instability in the context of plasma expansion, we first use 1D2V relativistic collisionless particle-in-cell (PIC) simulations, for which $\boldsymbol{k}=k_x\boldsymbol{e}_x$, and $\boldsymbol{B}=B_z\boldsymbol{e}_z$. Initially, ions occupy a slab of thickness $L=50c/\omega_{pe}$, while electrons are in Maxwell-Boltzmann equilibrium with the self consistent electrostatic potential. A vacuum region extends for about $2500c/\omega_{pe}$ on each side of the slab. The mass ratio is $m_e/m_i=1836$ with $Z=1$, and the electron temperatures are $T_{\perp 0}=T_{\parallel 0}=5$ keV. The code is run with a time step $\Delta t=0.2\omega_{pe}^{-1}$, a mesh size $\Delta x\approx c\Delta t$, and there are 2×10^4 particles in each mesh.

Figure 2(a) displays the time evolution of the total longitudinal ($E_k^\parallel$) and transverse ($E_k^\perp$) kinetic energies, and of the total magnetic energy (E_M). It shows that the global anisotropy $E_k^\perp/E_k^\parallel-1$ rises as the plasma expands. At $t=t_0\approx 28\omega_{pi}^{-1}$, the magnetic energy starts to increase, which indicates that the anisotropy is sufficient for the Weibel instability to grow. Then, for $t>t_i\approx 40\omega_{pi}^{-1}$, the magnetic field drives the isotropization of the electron temperature, which eventually leads to the saturation of the instability at $t\approx 48\omega_{pi}^{-1}$. According to Eq. (1), unstable modes should develop as soon as $k_x^m\geq 2\pi/L$, that is $A\geq 0.016$ for $L=50c/\omega_{pe}$. If one estimates the anisotropy based on the mean kinetic energies, the instability should start to grow around $\omega_{pi}t=4$, which is inconsistent with Fig. 2(a). To understand this discrepancy, we focus on Fig. 2(b), where A and B_z are plotted as a function of x, at $\omega_{pi}t=40$. The anisotropy is observed to be much larger on the sides of the plasma than in its center (the limit between these two parts being the rarefaction front). This is because the center of the plasma is mainly occupied by slow electrons which do not give any energy to ions (see Fig. 3 in Ref. [20]). As a result of this inhomogeneous anisotropy, unstable modes grow on the sides of the plasma, as shown by Fig. 2(b).

We now take into account this effect to determine when the instability is triggered. We assume that the expansion is

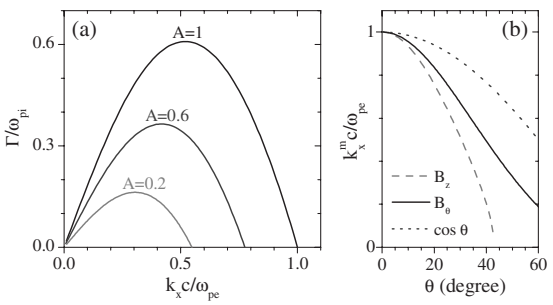

FIG. 1. Growth rate and maximum wave vector of the Weibel instability. (a) Growth rate Γ as a function of k_x for 3 different anisotropy parameters A and $T_{\perp 0}=5$ keV. (b) Maximum wave vector of the unstable modes B_z and B_θ, as a function of the angle between $\boldsymbol{k}$ and the plasma normal $\boldsymbol{e}_x$, for $A=1$.

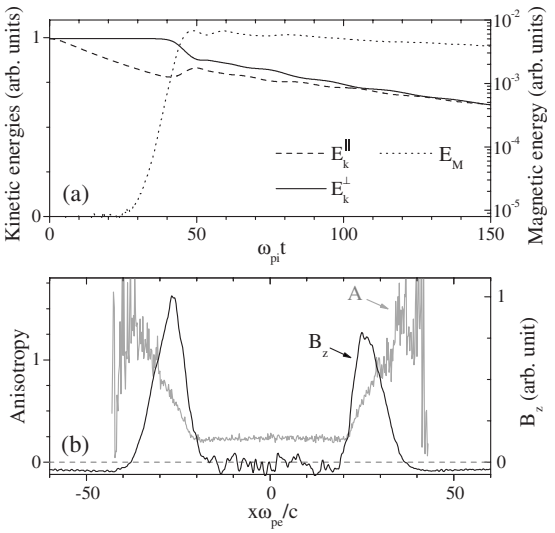

FIG. 2. Growth of the Weibel instability during a 1D2V expansion. (a) Integrated kinetic $(E_k^{\perp}, E_k^{\parallel})$ and magnetic (E_M) energies as a function of time, in linear and logarithmic scales, respectively. The same normalization is used for both E_k and E_M. (b) Anisotropy parameter A and magnetic field B_z as a function of space, at $\omega_{pi}t=40$.

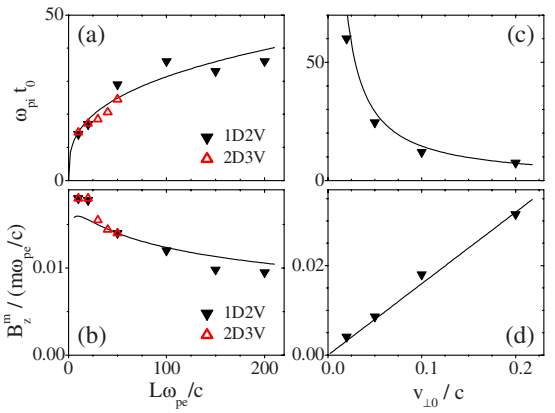

FIG. 3. (Color online) Simple model. (a-b) Influence of the plasma width L on the triggering time of the instability t_0, and on the peak magnetic field B_z^m, for $v_{\perp 0}=0.1c$. (c-d) Influence of the initial thermal velocity $v_{\perp 0}$ on t_0 and B_z^m, for $L=10c/\omega_{pe}$. The dots result from PIC simulations.

self-similar and that the width of the part of the plasma on which the instability grows is $L_A=\beta c_s t$, where $c_s=(k_B T_{\parallel 0}/m_i)^{1/2}$ is the ion acoustic velocity and $\beta\approx 3$ is chosen to reproduce simulation results [see e.g., Fig. 2(b)]. Then we use results of Refs. [20,21], to obtain an estimate of the anisotropy A around the center of mass of the anisotropic area (at $x=\pm L/2$). According to these papers the distribution function in the expansion direction is, to first order in t,

$$f_a^{\parallel}(x,v,t)\approx[1+(4-8u/3)uc_s t/L]f_{e0}^{\parallel}(v) \tag{2}$$

where $f_{e0}^{\parallel}(v)$ is the initial Maxwellian distribution function, $u=[m_e v_{\parallel}^2/2-e\Phi(x,t)]k_B T_{\parallel 0}$ the normalized total electron energy, and $\Phi(x,t)=-[1+(|x|-L/2)/c_s t]k_B T_{\parallel 0}/e$ the electrostatic potential. From Eq. (2), the longitudinal temperature $T_{\parallel}(t)$ is computed by averaging $m_e v_{\parallel}^2$ over $f_e^{\parallel}$. For $x=\pm L/2$, the potential is $\Phi(x,t)=-k_B T_{\parallel 0}/e$, and the averaging leads to $T_{\parallel}(t)\approx T_{\parallel 0}(1-\alpha c_s t/L)$ with $\alpha=32/3$. Thus the anisotropy for $t\ll L/c_s$ is $A=T_{\perp 0}/T_{\parallel}(t)-1\approx \alpha c_s/L$. Note that in Fig. 2(b), A is slightly lower than $\alpha c_s t/L$ because at this time it has stopped to increase.

The instability starts to grow when $2\pi/L_A=k_x^m$, that is when $2\pi/\beta c_s t=\sqrt{\alpha c_s t/L\omega_p/c}$. From this condition, we derive the triggering time of the instability,

$$t_0=\omega_{pi}^{-1}\frac{c}{v_{\perp 0}}\left(\frac{\pi^2\omega_{pe}L}{\alpha\beta c}\right)^{1/3}, \tag{3}$$

where $v_{\perp 0}=(k_B T_{\perp 0}/m_e)^{1/2}$. Figures 3(a) and 3(c) show that this simple formula reproduces quite well PIC simulation results, for different values of L and $v_{\perp 0}$.

This analysis can be pushed further to obtain an estimate of the peak magnetic field. We first compute the maximal current j_y^m that can be driven by the instability. To this end, the electron distribution function $f_e\propto\exp(-m_e v_{\parallel}^2/2k_B T_{\parallel}-m_e v_{\perp}^2/2k_B T_{\perp})$ is divided in isotropic and anisotropic parts, $f_e=f_e^0+f_e^A$, with $f_e^0\propto\exp(-m_e v^2/2k_B T_{\parallel})$. The magnetic field does not perturb f_e^0. In contrast, it deflects electrons associated to f_e^A in different directions, depending on the sign of their transverse velocity v_y. Actually, for $B_z>0$ the Lorentz longitudinal force $-ev_y B_z/m$, pushes electrons with $v_y<0$ in the positive x direction, and electrons with $v_y>0$ in the opposite direction. At most, all electrons of f_e^A with $v_y<0$ (respectively $v_y>0$) can pull out of a part of the plasma where they are replaced by electrons with $v_y>0$ (respectively, $v_y<0$), resulting in the local distribution function $f_e^m=f_e^0+2H(\pm v_y)f_e^A$, where H is the heaviside step function. The peak current j_y^m is simply obtained by averaging $-ev_y$ over f_e^m,

$$j_y^m=n_e e v_{\perp 0}\sqrt{2/\pi}[1-(A+1)^{-1/2}]. \tag{4}$$

For the sake of simplicity, we now approximate n_e by its mean value over L_A ($n_e\approx n_{e0}/\beta$, where n_{e0} is the total initial electron density), and we assume that j_y is sinusoidal. As both j_y and B_z vanish on the sides of L_A, B_z must be of the form $B_z^m[1+\cos k_x^m(x-x_0)]/2$ were $B_z^m=2\mu_0 j_y^m/k_x^m$, and x_0 is the center of the anisotropic area. Substituting for j_y^m, we get

$$B_z^m=\frac{2}{\beta}\sqrt{\frac{2}{\pi}}\frac{m\omega_{pe}}{e}\frac{v_{\perp 0}}{c}A^{-1/2}[1-(A+1)^{-1/2}]. \tag{5}$$

This function is plotted in Fig. 3(b) and 3(d) for $A=\alpha c_s t_0/L$, together with PIC results. The agreement is surprisingly good, considering the crude approximations made. Equation (5) actually provides both the order of magnitude of B_z^m and its behavior with L and $v_{\perp 0}$. We remark in particular that B_z^m depends weakly on L. For a given temperature, the maximum field is $B_z^{\max}/(m_e\omega_{pe}/e)\approx 0.16 v_{\perp 0}/c$, that is $B_z^{\max}\approx 20 v_{\perp 0}/c$ MG, for $n_{e0}=10^{21}$ cm^{-2}. Note that during the expansion, the magnetic layer always occupies the area between the rarefaction front and the vacuum. After the saturation of the instability, the amplitude of B_z thus tends to decrease.

Up to now we have not discussed the growth rate of B_z.

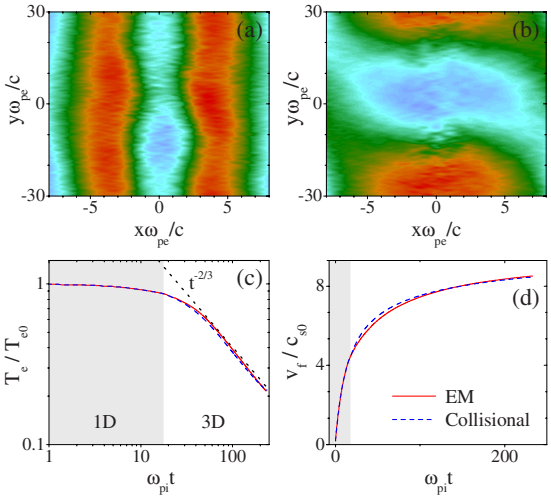

FIG. 4. (Color online) 2D3V simulations. (a) Magnitude of $\boldsymbol{B}$, at $t=26\omega_{pi}^{-1}$. From blue (light gray) to red (dark gray), $|\boldsymbol{B}|$ increases up to $0.018m_e\omega_{pe}/e$. (b) Angle θ between $\boldsymbol{B}$ and $\boldsymbol{e}_y$ in the $(\boldsymbol{e}_y,\boldsymbol{e}_z)$ plane. It goes from 80 degrees (light blue) up to 160 degrees (dark red). (c), (d) Electron temperature and ion front velocity as a function of time. The straight line is the result of an electromagnetic collisionless simulation, and the dashed line of an electrostatic collisional one. Collisions are inhibited in the gray area.

From Eq. (3) and the definition of A, we find that $A(t_0) \propto L^{-2/3}$, which means that the instability is triggered by smaller anisotropy for large L. According to Fig. 1(a), the field should therefore grow more slowly when L increases. This effect is clearly seen in PIC simulations. We also checked that the growth rates provided by these simulations are consistent with theoretical values. For $L=50c/\omega_{pe}$ for instance, we have at $t=40\omega_{pi}^{-1}$, $L_A=12c/\omega_{pe}$ and we estimate from Fig. 2 that $A\approx 0.6$. Figure 1 indicates that for $A=0.6$ and $k=2\pi/L_A=0.52\omega_{pe}/c$, $\Gamma=0.33\omega_{pe}$, which is close to the value directly measured in PIC simulation $\Gamma_{PIC}=0.3\omega_{pe}$.

Before concluding this 1D analysis, we note that Eqs. (3) and (5) are valid only if t_0 is smaller than the disassembly time $\tau=L/2c_s$. For very small L the rarefaction wave can reach the center of the plasma before the instability grows. In this case B_z develops in the whole plasma, and the model has to be slightly modified. The length under which this happens is computed from Eq. (3), and is given by $L_0=\pi/2(c/\omega_{pe})$, that is $L_0\approx 260$ nm for $n_{e0}=10^{21}$ cm^{-2}.

We now turn to two-dimensional in space and three-dimensional velocity (2D3V) simulations. The plasma is a semi-infinite slab with $L=20c/\omega_{pe}$ and 500 particles by cell, surrounded on both sides by $600c/\omega_{pe}$ of vacuum ($\Delta t=\Delta x/c=0.2\omega_{pe}^{-1}$). Periodic conditions for both the fields and the particles are used in the transverse direction (y axis), which is $L_y=60c/\omega_{pe}$ width. Figure 4(a) displays the magnitude of the magnetic field in the (x,y) plane, when it is maximum. It shows that $\boldsymbol{B}$ develops on the two sides of the plasma, just as in 1D2V simulations, and reaches the same peak value $B^m\approx 0.018m_e\omega_{pe}/e$ as in 1D. The growth of $\boldsymbol{B}$ starts at the same time $t_0\approx 17\omega_{pi}^{-1}$ in the two cases. This indicate that Eqs. (3)–(5) are still valid in $2D$, which is confirmed by additional simulations [see Figs. 3(a) and 3(b)].

There is however a significant difference between 1D and two-dimensional (2D) simulations, as shown by Fig. 4(b): in 2D the orientation of $\boldsymbol{B}$ depends on y, which means that some modes grow with nonpurely longitudinal wave vectors. For instance in the case of Fig. 4, the magnetic field is made of three main modes and can be approximated by

$$\boldsymbol{B} \approx [B_1\boldsymbol{e}_z + B_2\cos k_y(y-y_0)\boldsymbol{e}_\phi]\cos k_x(x-x_0), \qquad (6)$$

with $B_1\approx 0.013m_e\omega_{pe}/e$, $B_2\approx 0.004m_e\omega_{pe}/e$, $\boldsymbol{e}_\phi=\cos\phi\,\boldsymbol{e}_y+\sin\phi\,\boldsymbol{e}_z$, $\phi\approx 52°$, $k_x\approx\omega_{pe}/c$, and $k_y=0.1\omega_{pe}/c$. This shows that the plasma supports two non-longitudinal modes which have wave vectors making an angle of $\theta\approx\pm 5.7°$ with the x-axis. The existence of such modes is not surprising. Actually, since for small angles $k_x^m(\theta)\approx k_x^m(0)$ [see Fig. 1(b)], these modes are triggered at the same time t_0 than longitudinal modes. In contrast, large angle modes are forbidden because they require larger anisotropy to grow. As A begins to decrease soon after t_0, such modes can indeed never be triggered. To check this analysis, we performed simulations with different transverse width L_y, and we observed that for $L_y<36c/\omega_{pe}$, i.e., $\theta_{\min}\gtrsim 10°$, only longitudinal modes develop. As in realistic cases, the transverse width of the plasma is much larger than $36c/\omega_{pe}$, modes with $\theta>0$ can generally grow during the expansion.

In general, the orientation of the magnetic field therefore varies in the transverse directions. Unexpectedly, this effect simplifies the physics of the expansion, avoiding the trapping of particles, which occurs in 1D2V and some 2D geometries [14–17]. As a result, though the magnetic field drives complex electron trajectories, its only macroscopic effect is to isotropize the electron temperature. This isotropization is effective as soon as the cyclotron frequency $\omega_c^m=eB^m/m_e$ is greater than the inverse of the expansion characteristic time $2c_s/L$, that is $L\gtrsim 0.3c/\omega_{pe}$. When this condition is fulfilled, the expansion is divided in two stages: while $t\leq t_0$ electrons transfer only their longitudinal energy to ions, then at the time t_i which is of the order of t_0, they start to deliver also their transverse energy, and the expansion becomes isotropic $[T_\perp=T_\parallel=T_e(t), \forall t\geq t_i]$.

To check that this is the only macroscopic effect of $\boldsymbol{B}$, we compare in Figs. 4(c) and 4(d), the evolution in time of the electron temperature and of the ion front velocity, obtained when $L_y=60c/\omega_{pe}$, with the ones provided by a 2D3V electrostatic collisional code. In this code, the thermal collision frequency was forced to $\nu=0.3(v/v_{\perp 0})^{-3}\omega_{pe}$, which is, according to Ref. [10], sufficient to ensure an isotropic expansion. Further, to mimic the electromagnetic simulation, we inhibited the collisions for $t<t_i=17.4\omega_{pi}^{-1}$. In Figs. 4(c) and 4(d), the agreement between the two codes is almost perfect, indicating that the magnetic field has the same influence on the expansion as do elastic Coulomb collisions. We note in particular in Fig. 4(c) that T_e decreases as $t^{-2/3}$, instead of t^{-2} in the purely 1D case. This is because ions take their energy from both the longitudinal and the transverse directions [10]. This important result shows that if the plasma is sufficiently thick ($L\gtrsim 0.3c/\omega_{pe}$), ions will always end up taking all the electron energy, just as if the plasma was collisional.

We now briefly discuss the case of ion acceleration on the rear side of thin targets interacting with intense laser pulses [11]. The electron distribution in this case generally differs

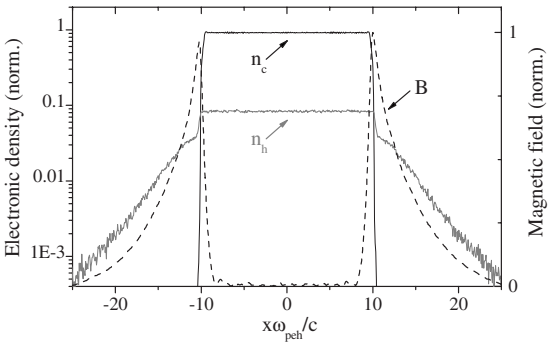

FIG. 5. Growth of the Weibel instability in a bi-Maxwellian plasma. The electronic densities n_h and n_c are plotted together with B, at $t=35\omega_{pih}^{-1}$. In this 1D simulation, we took $T_{h0}/T_{c0}=100$ with $T_{h0}=5$ keV, $f_h=0.1$, and $L=20c/\omega_{peh}$.

from a Maxwellian, because a large number of electrons are accelerated by the laser. To take into account this energetic tail, the plasma is generally modeled by a bi-Maxwellian distribution with a cold population that describes thermal electrons, and a hot population associated with accelerated electrons. To facilitate the comparison with the one-temperature case, we define the partial electron (ion) plasma frequency $\omega_{peh}=f_h^{1/2}\omega_{pe}$ $(\omega_{pih}=f_h^{1/2}\omega_{pi})$ and the partial ion acoustic velocity $c_{sh}=(Zk_BT_{h0}/mi)^{1/2}$. In the following, we consider that the fraction of hot electrons is small $f_h=n_h/(n_h+n_c)\ll 1$, and that the cold temperature is steady (this is supported by Fig. 8 in Ref. [9]). Under this last condition, we easily derive a new dispersion relation, from which we find that unstable modes have wave vectors $k_x<k_c^m=(f_hA)^{1/2}$. This shows that cold electrons tend to stabilize the plasma. For this reason, the magnetic field in a bi-Maxwellian plasma develops only in its "hot-dominated" part, as illustrated by Fig. 5.

If $T_h/T_c\gg 1$, we can neglect the motion of cold electrons, and assume that the length of the anisotropic layer is $L_A=2c_{sh}t$ (that is $\beta=2$ rather than $\beta=3$). Doing so we find that the triggering time is slightly increased by the presence of a cold population. The agreement between the model and PIC simulations is still quite good. In the case of Fig. 5 for instance, we measured $\omega_{pih}t_0=21$ in agreement with Eq. (3). Note that in a bi-Maxwellian plasma, this equation is valid even for very small L because the rarefaction wave which is mainly governed by cold electrons is very slow [9]. If Eq. (3) fits well PIC results, Eq. (5) significantly underestimates B^m. This is probably because B deviates strongly from a sine. Be that as it may, we observed that the maximum magnetic field is enhanced by the presence of cold electrons. For example, in the case of Fig. 5 we measured $B^m\approx 0.033m_e\omega_{peh}/e\approx 4$ MG for $n_{e0h}=10^{21}$ cm^{-2}, instead of $B^m\approx 2$ MG with only hot electrons.

In conclusion, high-amplitude magnetic fields can develop at the surface of plasma slabs expanding into a vacuum. This phenomenon has important repercussions on the plasma expansion. In particular, the self-generated magnetic fields can keep the electron distribution isotropic during the expansion. Coulomb collisions can have a similar effect, but according to Ref. [10], the collisional isotropization is effective only when $(n_e/10^{19}\ \text{cm}^2)(L/\mu\text{m})/(T_e/\text{eV})^2\gtrsim 1$. As a result magnetic fields are much more efficient than collisions to transfer the electron transverse energy to ions in a moderately dense and warm plasma. We showed that the presence of a cold electron population does not affect significantly the development of the Weibel instability. This study in the outer plasma can, therefore, apply to the specific case of ion acceleration at the rear side of a thin foil irradiated by an intense laser pulse. Similar effects should also occur in dusty or magnetized plasmas. In this last case, the presence of a static magnetic field B_0 should influence both t_0 and B^m, for k_x^m is a function of B_0 [12].

We gratefully acknowledge T. M. Antonsen for helpful discussions and remarks on the manuscript. This work was partly supported by the AXA Research Fund and by Agence Nationale de la Recherche under Project No. ANR-06-BLAN-0392.

[1] U. Samir, K. H. Wright, Jr., and N. H. Stone, Rev. Geophys. Space Phys. **21**, 1631 (1983).
[2] K. E. Lonngren, Planet. Space Sci. **38**, 1457 (1990).
[3] R. A. Snavely *et al.*, Phys. Rev. Lett. **85**, 2945 (2000).
[4] E. L. Clark *et al.*, Phys. Rev. Lett. **84**, 670 (2000).
[5] A. Maksimchuk, S. Gu, K. Flippo, D. Umstadter, and V. Y. Bychenkov, Phys. Rev. Lett. **84**, 4108 (2000).
[6] R. K. Singh and J. Narayan, Phys. Rev. B **41**, 8843 (1990).
[7] A. V. Gurevich, L. V. Pari ĭ skaya, and L. P. Pitaevski ĭ , Zh. Eksp. Teor. Fiz. **49**, 647 (1965).
[8] P. Mora, Phys. Rev. Lett. **90**, 185002 (2003).
[9] P. Mora, Phys. Rev. E **72**, 056401 (2005).
[10] C. Thaury, P. Mora, J. C. Adam, and A. Héron, Phys. Plasmas **16**, 093104 (2009).
[11] S. C. Wilks, A. B. Langdon, T. E. Cowan, M. Roth, M. Singh, S. Hatchett, M. H. Key, D. Pennington, A. MacKinnon, and R. A. Snavely, Phys. Plasmas **8**, 542 (2001).
[12] E. S. Weibel, Phys. Rev. Lett. **2**, 83 (1959).
[13] K. Bendib, A. Bendib, and A. Sid, Laser Part. Beams **16**, 473 (1998).
[14] R. L. Morse and C. W. Nielson, Phys. Fluids **14**, 830 (1971).
[15] H. H. Kaang, C.-M. Ryu, and P. H. Yoon, Phys. Plasmas **16**, 082103 (2009).
[16] A. Stockem, M. E. Dieckmann, and R. Schlickeiser, Plasma Phys. Controlled Fusion **51**, 075014 (2009).
[17] L. Palodhi, F. Califano, and F. Pegoraro, Plasma Phys. Controlled Fusion **51**, 125006 (2009).
[18] D. V. Romanov, V. Y. Bychenkov, W. Rozmus, C. E. Capjack, and R. Fedosejevs, Phys. Rev. Lett. **93**, 215004 (2004).
[19] A. Bret, M.-C. Firpo, and C. Deutsch, Phys. Rev. E **70**, 046401 (2004).
[20] T. Grismayer, P. Mora, J. C. Adam, and A. Héron, Phys. Rev. E **77**, 066407 (2008).
[21] P. Mora and T. Grismayer, Phys. Rev. Lett. **102**, 145001 (2009).